Ultra-Wideband-Based Localization for Quadcopter Navigation

Article · February 2016

DOI: 10.1142/S2301385016400033

7 authors, including:

Kexin Guo
Nanyang Technological University
15 PUBLICATIONS **88** CITATIONS
SEE PROFILE

Zhirong Qiu
Nanyang Technological University
20 PUBLICATIONS **188** CITATIONS
SEE PROFILE

Abdul Hanif Zaini
Nanyang Technological University
10 PUBLICATIONS **71** CITATIONS
SEE PROFILE

Wei Meng
National University of Singapore
35 PUBLICATIONS **405** CITATIONS
SEE PROFILE

Unmanned Systems, Vol. 4, No. 1 (2016) 23–34

DOI: 10.1142/S2301385016400033

UNMANNED SYSTEMS
http://www.worldscientific.com/worldscinet/us

Ultra-Wideband-Based Localization for Quadcopter Navigation

Kexin Guo[*,§], Zhirong Qiu[*,¶], Cunxiao Miao[‡,‖], Abdul Hanif Zaini[*,**], Chun-Lin Chen[*,††], Wei Meng[†,‡‡], Lihua Xie[*,§§]

[*]*Nanyang Technological University, Singapore 639798*

[†]*National University of Singapore, Singapore 117411*

[‡]*University of Science and Technology Beijing, Beijing 100083, P. R. China*

Micro unmanned aerial vehicles (UAVs) are promising to play more and more important roles in both civilian and military activities. Currently, the navigation of UAVs is critically dependent on the localization service provided by the Global Positioning System (GPS), which suffers from the multipath effect and blockage of line-of-sight, and fails to work in an indoor, forest or urban environment. In this paper, we establish a localization system for quadcopters based on ultra-wideband (UWB) range measurements. To achieve the localization, a UWB module is installed on the quadcopter to actively send ranging requests to some fixed UWB modules at known positions (anchors). Once a distance is obtained, it is calibrated first and then goes through outlier detection before being fed to a localization algorithm. The localization algorithm is initialized by trilateration and sustained by the extended Kalman filter (EKF). The position and velocity estimates produced by the algorithm will be further fed to the control loop to aid the navigation of the quadcopter. Various flight tests in different environments have been conducted to validate the performance of UWB ranging and localization algorithm.

Keywords: UWB ranging; localization; GPS-denied environments; EKF; quadcopters.

US

1. Introduction

Recent years have witnessed the surge of research interest on micro unmanned aerial vehicles (UAVs). As the logical heir of ground based mobile robots, UAVs have the aerial maneuvering ability to easily avoid obstacles and acquire an excellent bird's-eye view, which provides a great convenience in mapping and monitoring tasks [1]. At a small size, micro UAVs are able to navigate through spatially restricted areas, such as forests [2], urban canyons [3] and indoor environments [4], while still maintaining the lowest disturbance to environment and the inhabitants within. It can be reasonably expected that micro UAVs are about to play more and more important roles for both civilian and military purposes [5], like reconnaissance for search and rescue [6], environment monitoring [7], security surveillance [8], inspection [9], law enforcement [10], etc. Specifically, quadcopters are selected to be the universal research platform due to its low cost and availability of various sizes as well as easy maintenance.

Precise localization is critical in achieving the autonomous navigation of micro UAVs. In an outdoor environment, space-based satellite navigation systems such as Global Positioning System (GPS) are able to provide an absolute position for the UAV with an approximate error of 2–5 m in civilian applications. With a ground-based reference station installed at a known position, Differential-GPS is able to achieve less than 1 m overall accuracy. To improve the accuracy, the position provided by a satellite navigation system is usually fused with Inertial Measurement Unit (IMU) [11, 12], which contains measurements from accelerometers, gyroscopes and sometimes also magnetometers. Other localization methods are based on vision [13–15] or a combination of vision and IMU.

However, in a spatially restricted area or dense environment, say woods or urban canyons, GPS signals will

Received 22 October 2015; Revised 22 November 2015; Accepted 23 November 2015; Published 5 February 2016. This paper was recommended for publication in its revised form by Special Issue Guest Editor, Lu Liu.
Email Addresses: [§]*guok0005@e.ntu.edu.sg*, [¶]*qiuz0005@e.ntu.edu.sg*, [‖]*miao_cunxiao@163.com*, [**]*e150010@e.ntu.edu.sg*, [††]*chencl@ntu.edu.sg*, [‡‡]*tslmeng@nus.edu.sg*, [§§]*elhxie@ntu.edu.sg*

suffer greatly from the blocking of line-of-sight and multipath effects, and the localization accuracy degrades to a level that it can no longer support autonomous flight. Furthermore, GPS units are unable to work in an indoor environment. In this case, some other anchor-based localization systems [16] are needed to replace the GPS for the navigation of UAV. Typically, anchors are placed at points with known coordinates, and the distance from an anchor to the moving UAV can be estimated from RF signals for the localization purpose. Different kinds of ranging techniques have been proposed for the distance estimation [17, 18]: Time of Flight (ToF), Time of Arrival (ToA) and Received Signal Strength Indication (RSSI).

One emergent RF technology for accurate localization is ultra-wideband (UWB) ranging technology, which is robust to multipath and nonline-of-sight (NLOS) effects, and can achieve a cm-level ranging error. The UWB radio modules can estimate inter-module distance by measuring the transmission and reception time of UWB pulses [19–21]. In contrast with other RF systems, UWB pulses can be transmitted between 3 GHz and 5 GHz and have an RF bandwidth of 1.4 GHz. The increased bandwidth not only avoids the interference with other types of RF signals, e.g. remote control and WiFi signals but also allows the UWB signal to easily go through walls and other obstacles. Besides, the ultra-short duration pulses permit an easy filtering method to deal with the multipath effect, as well as an accurate determination of ToF. Some commercial UWB systems exploit a peer-to-peer Two-Way Time of Flight (TW-ToF) to simultaneously achieve precise ranging and data exchange, which potentially provides more information for localization.

In this paper, we employ UWB modules for the localization of quadcopters in GPS-denied environments. The UWB module on the moving quadcopter is to actively send ranging requests to anchor UWB nodes at known positions to obtain the distance measurements, which will be fused by the extended Kalman filter (EKF) for position estimation. Moreover, an estimated position will be fed into the navigation unit of the quadcopter to aid the navigation. Various experiments in different environments have been conducted to verify the performance of the UWB localization.

The remainder of this paper is organized as follows. The TW-ToF ranging technique and calibration of the UWB rangings are introduced in Sec. 2. After that, a UWB localization algorithm is proposed in Sec. 3. The hardware configuration of the navigation system is shown in Sec. 4, and an experiment evaluation of the UWB localization in different environments, as well as related autonomous quadcopter flight in an indoor environment, is presented in Sec. 5. We conclude our work in Sec. 6.

The following notations will be used throughout this paper. M^T denotes the transpose of the matrix M. $A \otimes B$ is the Kronecker product of the two matrices A and B. $||v||$ is the two-norm of the vector v. $\mathrm{diag}(a_1, \ldots, a_n)$ denotes the diagonal matrix with the diagonal elements given by $a_1, \ldots, a_n$.

2. Two-Way Time-of-Flight Ranging and Calibration of UWB Measurement

In this section, we shall introduce the TW-ToF ranging technique implemented on the UWB module for the localization in GPS-denied environments. Besides, we shall also discuss the calibration of UWB measurement.

2.1. *Two-way time-of-flight ranging*

Unlike ultrasonic or laser-based signals, UWB pulses can travel through walls and dense foliage. Compared with conventional narrow-band RF, these pulses do not suffer from errant multi-path reflections since the most direct path through the environment is measured based on TW-ToF technique (Fig. 1).

It is clear from Fig. 1, that the two UWB modules involved in ranging are asymmetrical. Specifically in our localization context, the module installed on the quadcopter (denoted as Q) will actively send its ranging request to the anchor module at known position (denoted as A). The anchor will automatically respond to any ranging request it receives from the requester. As shown in Fig. 1, the onboard UWB module Q initiates the TW-ToF by transmitting a request packet at $Q_{M_0}^{T_x}$. Anchor A receives the pulse at $A_{M_0}^{R_x}$ after a delay of f. After calculating the leading edge offset with a known delay δ_A, anchor A responds by transmitting a pulse at $A_{M_1}^{T_x}$. Q receives it after a delay of f at $Q_{M_1}^{R_x}$. The pulse transmission time f between Q and A is calculated by

$$f = \frac{(Q_{M_1}^{R_x} - Q_{M_0}^{T_x} - \delta_A)}{2}.$$

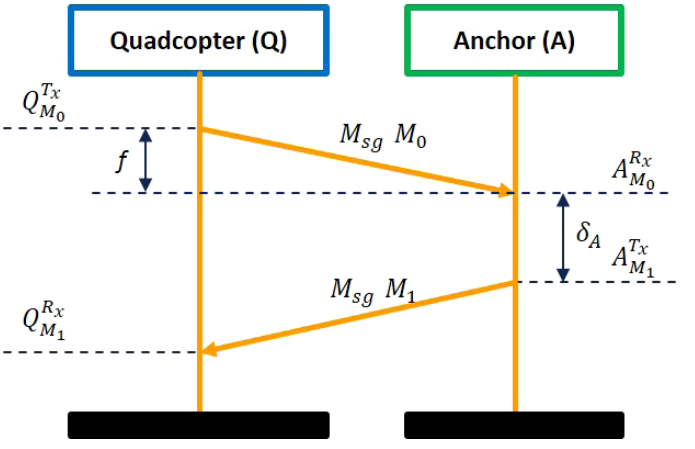

Fig. 1. TW-ToF range measurement.

Furthermore, the range d_{QA} between Q and A is given by

$$d_{QA} = f * c,$$

where c is the speed of light in vacuum with the approximate constant of 3×10^8 m/s.

2.2. *Calibration of UWB measurement*

Here, we discuss a methodology to calibrate the UWB but defer the experiment results to Sec. 5.1. Assume that a UWB range r has been obtained, which can be modeled as a simple linear function of the true distance d. More exactly, if we take into account the zero-mean random error ϵ, then the following holds:

$$r = ad + b + \epsilon. \tag{1}$$

The calibration problem is to estimate d from the range r.

The classical approach is adopted for the calibration, which firstly regresses the instrumental response r on the manipulated variable d and then solves for d. Specifically, given n samples (d_i, r_i), $i = 1, \ldots n$ collected from different locations, the calibration can be conducted as follows [22]. Linear regression is firstly applied to n samples to obtain an estimate $\hat{a}, \hat{b}$, respectively, for scaling factor a and bias b in the measurement model (1) as well as an estimate $\hat{\sigma}$ of the standard deviation of the error ϵ:

$$\begin{aligned} \hat{a} &= \frac{\sum_{i=1}^{n}(d_i - \bar{d})(r_i - \bar{r})}{\sum_{i=1}^{n}(d_i - \bar{d})^2}, \\ \hat{b} &= \bar{r} - \hat{a}\,\bar{d}, \\ \hat{\sigma} &= \frac{\sum_{i=1}^{n}(r_i - \hat{a}d_i - \hat{b})^2}{n-2}, \end{aligned} \tag{2}$$

where $\bar{d}$ and $\bar{r}$ are, respectively, the mean of d_i's and r_i's, $i = 1, \ldots, n$. After that, the ranging estimate $\hat{d}$ can be obtained as

$$\hat{d} = \tilde{a}\hat{r} + \tilde{b}, \tag{3}$$

with $\tilde{a} = \frac{1}{\hat{a}}$ and $\tilde{b} = -\frac{\hat{b}}{\hat{a}}$. It can be shown that [23] the estimate is asymptotically unbiased and normal in the case of a normal error ϵ, and the asymptotic mean square estimation error is approximated by

$$R = (\hat{\sigma}/\hat{a})^2. \tag{4}$$

3. UWB-Based Localization

The workflow of the UWB localization system is displayed in Fig. 2. To achieve the range-based localization, anchor nodes equipped with UWB module are firstly installed at known positions. As the TW-ToF ranging method described in Sec. 2.1, the UWB module on the quadcopter is to actively send ranging requests to anchor nodes for distance measurement. Once a distance is obtained, it will be calibrated by (3) where the calibration parameters $\tilde{a}$ and $\tilde{b}$ are determined by experiments as shown later in Sec. 5.1. The calibrated range then goes through the outlier detection before it is fed into a localization algorithm to produce a position estimate. Note that trilateration is used to start the algorithm, whose output will serve as the initial state estimate for EKF. The follow-up localization is sustained by EKF in a recursive way.

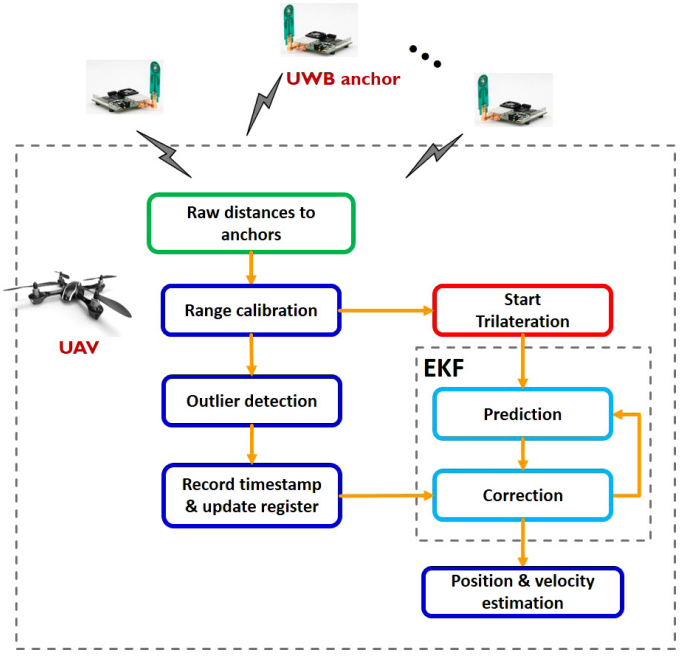

Fig. 2. UWB-based localization workflow.

Below, we shall elaborate each part of our UWB based localization system. In specific, the kinematic and measurement model is firstly presented, followed by a comparison of two major recursive Gaussian filters, namely EKF and Unscented Kalman Filter (UKF). The equations of EKF are introduced later, based on which the outlier detection is mentioned. The trilateration algorithm for the initialization phase is discussed finally.

3.1. *Kinematic and measurement model*

For the UWB localization, the position $p = (p_x, p_y, p_z)'$ and velocity $v = (v_x, v_y, v_z)'$ of the mobile node are to be estimated. Assume that the acceleration $a = (a_x, a_y, a_z)'$ remains constant in $[t_{k-1}, t_k]$, we can model the discrete-time

dynamics of the mobile node as

$$\begin{pmatrix} p \\ v \end{pmatrix}_{k+1} = \begin{pmatrix} I & \Delta t_k I \\ 0 & I \end{pmatrix} \begin{pmatrix} p \\ v \end{pmatrix}_k + \begin{pmatrix} \frac{1}{2} a_k (\Delta t_k)^2 \\ a_k \Delta t_k \end{pmatrix}. \quad (5)$$

In the case when the acceleration is not available, $\{a_k\}$ can be treated as a white noise sequence with the covariance $E(a_k a_k^T) = \mathrm{diag}(\sigma_x^2, \sigma_y^2, \sigma_z^2)$. Note that σ_π can be set as the maximum acceleration on the π-direction ($\pi = x, y, z$) for a conservative but consistent estimation.

On the other hand, the measurement equation is given by

$$d_k = ||p_k - p^a|| + \eta_k, \quad (6)$$

where d_k is the calibrated distance from the UWB ranging r_k by (3), $p^a = (x^a, y^a, z^a)$ is the anchor's position and η_k is the measurement noise whose variance R is given by (4). Note that the linearization around $\hat{p}_k$ can be written as $d_k \approx \hat{d}_k + \frac{1}{\hat{d}_k}(\hat{p}_k - p^a)^T(p - \hat{p}_k) + \eta_k$ and $\hat{d}_k = ||\hat{p}_k - p^a||$.

To sum up, the process dynamics and the measurement equation for the UWB localization can be found as

$$\begin{cases} x_{k+1} = A_k x_k + \varepsilon_k, & E(\varepsilon_k \varepsilon_k^T) = Q_k, \\ d_k = ||p_k - p^a|| + \eta_k, & E(\eta_k \eta_k^T) = R, \end{cases} \quad (7)$$

where $x = \begin{pmatrix} p \\ v \end{pmatrix}$, $A_k = \begin{pmatrix} I & \Delta t_k I \\ 0 & I \end{pmatrix}$ and $Q_k = \begin{pmatrix} \frac{1}{4}(\Delta t_k)^4 & \frac{1}{2}(\Delta t_k)^3 \\ \frac{1}{2}(\Delta t_k)^3 & (\Delta t_k)^2 \end{pmatrix} \otimes \mathrm{diag}(\sigma_x^2, \sigma_y^2, \sigma_z^2)$.

3.2. *Comparison of EKF and UKF*

The localization of moving objects is usually achieved by recursive Bayesian filters. Since the seminal paper of Rudolph Kalman [24], the Kalman filter has been widely used in the state estimation of discrete-time linear systems with Gaussian noise. It provides a recursive state estimation from measurements, and is also able to fuse asynchronous measurements from different sensors as well.

For a general nonlinear dynamics, two major types of extension of Kalman filter can be applied: EKF and UKF. EKF is obtained by implementing the Kalman filter in the linearized system, and it similarly consists of the prediction from the process equation and correction from the measurement, as shown later in Sec. 3.3. These two phases are also comprised in UKF, however, UKF employs the unscented transform to choose a set of sample points (sigma points) for the state and observation prediction, as well as the covariance propagation. Compared with EKF, UKF is capable in dealing with highly nonlinear dynamics due to the unscented transform; nonetheless, the choosing of sigma points relies on finding the matrix square root of the covariance, and hence entails more computational burden. In addition, the weights of sigma points have to be selected carefully and cannot be applied universally.

In the next, we compare the performance of EKF and UKF for the system (7) in localization. In detail, two different sets of anchors are set up in the simulation, one with the configuration as in the indoor environment (Sec. 5.3), and the other one as in the outdoor environment (Sec. 5.2). The sampling interval of UWB ranging is set as 0.1 s in both cases. In the UKF algorithm, the weights of sigma points are set as in [25]. In the indoor simulation, the tracked object is assumed to move along a circle with radius of 2 m at a certain height of 1.5 m, at a uniform linear velocity of 0.8 m/s; in the outdoor case, it is assumed to move along a circle with radius of 25 m at the same height, at a uniform linear velocity of 2 m/s.

Figures 3 and 4, respectively, show the simulation results of these two scenarios over 1000 steps of rangings. Clearly in both cases, EKF is able to track the object accurately for the x and y coordinate, along with some variation for z coordinate which is due to the anchor configuration. In fact,

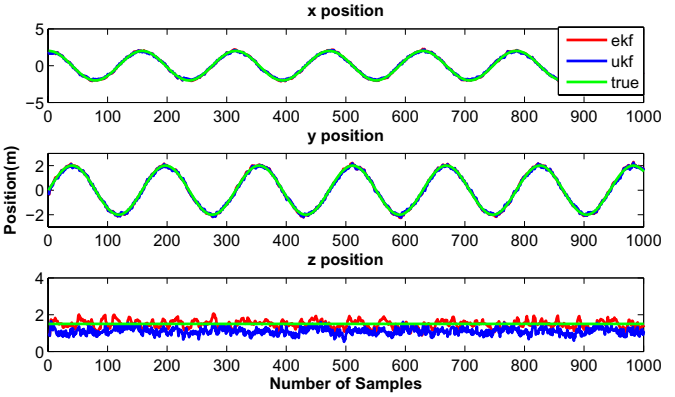

(a) EKF and UKF indoor position

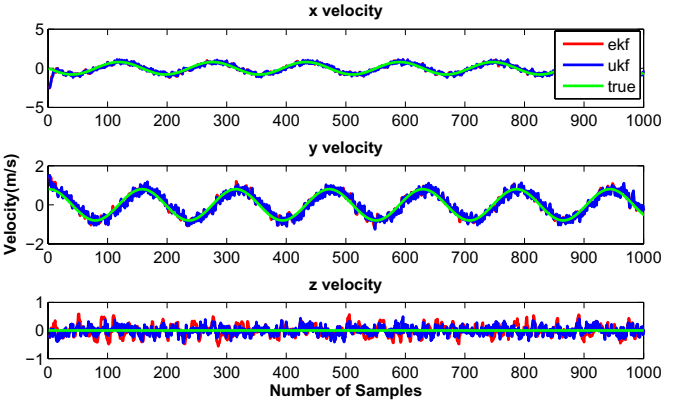

(b) EKF and UKF indoor velocity

Fig. 3. Indoor simulation results of EKF and UKF.

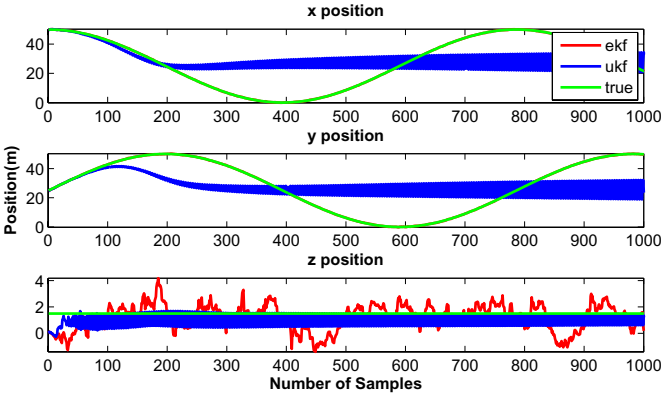

(a) EKF and UKF outdoor position.

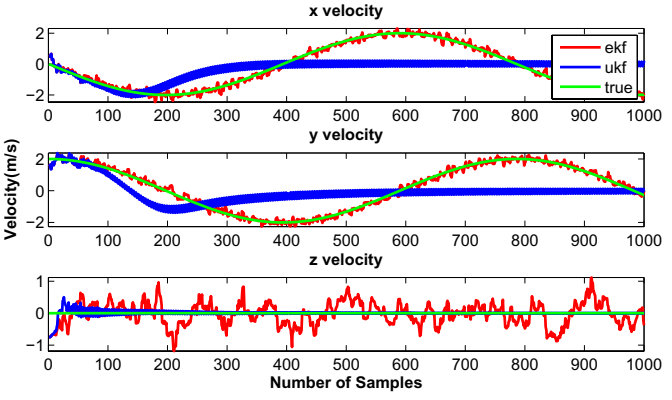

(b) EKF and UKF outdoor velocity.

Fig. 4. Outdoor simulation results of EKF and UKF.

note that in system (7) only the measurement equation is nonlinear; besides, with a small initial estimation error, EKF is expected to provide a consistent estimate [26]. In contrast, UKF can only perform similarly in the indoor simulation, but yields an inconsistent estimation in the outdoor case. It reveals the sensitivity of weights of sigma points of UKF to different anchor configurations. As a result, EKF is preferred for UWB-based localization system, and the corresponding algorithm is detailed in Sec. 3.3.

3.3. *EKF*

Applying the EKF to the system (7) yields the localization equations as in (8)–(13), with $\hat{x}_k^-$ and $\hat{x}_k$, respectively, being *a priori* and *a posteriori* estimate of the state at the time t_k, P_k^- and P_k the corresponding covariance of the estimation error.

Process update ("Prediction")

$$\hat{x}_k^- = A_{k-1}\hat{x}_{k-1}, \tag{8}$$

$$P_k^- = A_{k-1}P_{k-1}A_{k-1}^T + Q_{k-1}. \tag{9}$$

Measurement update ("Correction")

$$\begin{cases} \hat{d}_k = ||\hat{p}_k^- - p^a||, \\ H_k = \dfrac{1}{\hat{d}_k}\left[(\hat{p}_k^- - p^a)^T \quad 0\right]_{6\times 1}, \end{cases} \tag{10}$$

$$K_k = P_k^- H_k^T (H_k P_k^- H_k^T + R)^{-1}, \tag{11}$$

$$\hat{x}_k = \hat{x}_k^- + K_k(d_k - \hat{d}_k), \tag{12}$$

$$P_k = (I - K_k H_k)P_k^-. \tag{13}$$

It is clear that the implementation of the EKF above only requires a minimal amount of computation. Most of the calculation is from the matrix multiplication and addition. Although the Kalman gain update (11) involves a matrix inversion, it is actually a scalar division due to the scalar distance measurement. Therefore the real time localization is readily achieved.

3.4. *Outlier detection*

For UWB ranging modules, although the range measurement is accurate even in close proximity of strong reflectors like walls, there exist unreasonable data (e.g. negative distances or dramatic change between two consecutive samples) especially in NLOS environment like forest (Fig. 10(a)), as can be seen from Fig. 5. On the other hand, it is noted that the Kalman filter is not robust to measurement outliers, which is also true for EKF and results in erratic estimation. Therefore, it is necessary to let measurements go though outlier detection before applying them, which is

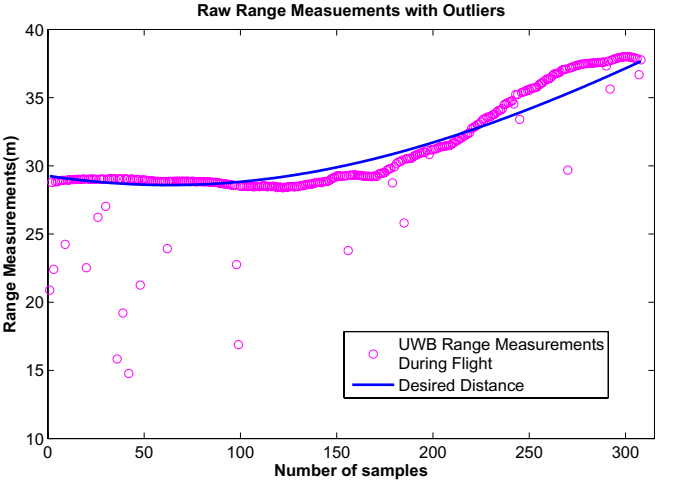

Fig. 5. Raw range data collected in forest environment.

completed by calculating the Mahalanobis distance related with the innovation covariance. Specifically, from (11) and (12), the innovation and its covariance are respectively given by $d_k - \hat{d}_k$ and $H_k P_k^- H_k^T + R$. As a result, the Mahalanobis distance [27] of the innovation is found as

$$D = (d_k - \hat{d}_k)(H_k P_k^- H_k^T + R)^{-1}(d_k - \hat{d}_k) = \frac{(d_k - \hat{d}_k)^2}{H_k P_k^- H_k^T + R}.$$

The larger the normalized distance D, the more likely the measurement is an outlier. Some threshold can be set for the detection.

3.5. *Trilateration*

Theoretically, trilateration method utilizes simultaneous distance measurements from several anchor nodes to determine the location of the mobile node. However, with the UWB ranging technique, these distances can only be retrieved in a cyclic fashion, which entails asynchrounous measurements and results in large localization error, especially when the mobile node is moving at a high speed. Hopefully, trilateration is still able to generate a rough estimate to initialize or restart the UWB localization.

As is known, it is necessary to obtain ranges from at least four noncoplanar anchors as well as their coordinates to uniquely determine the target position in a 3D space. Denote the known position of the ith anchor node as $p_i^a = (x_i^a, y_i^a, z_i^a)$ and the corresponding calibrated distance as d_i, then we have

$$d_i = \sqrt{(x - x_i^a)^2 + (y - y_i^a)^2 + (z - z_i^a)^2}, \quad i = 1, \ldots, n, \tag{14}$$

where (x, y, z) is the target location to be found.

Many different methods have been proposed to solve (14) [28–30]. Typically, it can be solved by a combination of linear and nonlinear least square methods [31]. In fact, by squaring both sides of (14) and subtracting

$$d_1^2 = (x - x_1^a)^2 + (y - y_1^a)^2 + (z - z_1^a)^2,$$

we get $n - 1$ linear equations as

$$d_i^2 - d_1^2 - d_{i1}^2 = 2[(x_1^a - x_i^a)x + (y_1^a - y_i^a)y + (z_1^a - z_i^a)z], \tag{15}$$

with $d_{i1}^2 = (x_i^a)^2 - (x_1^a)^2$, $i = 2, \ldots, n$, which can be solved by least squares. On the other hand, the nonlinear least squares problem related with (14), i.e.

$$\min_{(x,y,z)} \sum_{i=1}^{n} [d_i - \sqrt{(x - x_i^a)^2 + (y - y_i^a)^2 + (z - z_i^a)^2}]^2,$$

can be efficiently solved by Gauss–Newton method [32] with an acceptable initial guess provided by solving the linear least squares problem (15).

4. Hardware Configuration of the Experimental Quadcopter

In this section, we shall have an overview of the hardware configuration of the quadcopter used in experiments. The range calibration and UWB-based localization tests are carried out on a commercial low-cost frame of DJI F450 radio-controlled (RC) quadcopter, with its four motors replaced by the small and powerful AXI 2217/20 for endurance extension. All of the airborne modules are manufactured shown in Fig. 7(a). Three main electronic components constitute the on-board avionics (Fig. 7(b)): UWB module, BeagleBone Black (BBB) micro computer, and Pixhawk Autopilot [33].

The UWB platform for the experiment is Time Domain's P410 RCM (Fig. 6) with operating band from 3.1 GHz to 5.3 GHz. Within the the range of 125 m, it is able to provide precise measurement at an update rate of around 40 Hz. Its dimension (7.6 × 8.0 × 1.6 cm) and weight (58 g) are suitable for micro unmanned systems. The RF emission is compliant with the U.S. Federal Communications Commission (FCC) limits.

The BBB is a low-cost credit-card-sized development platform with good support including 512 MB RAM, 2 GB of eMMC flash on-board and ARM Cortex-A8 processor with speed of 1 GHz. The maximum power consumption is around 2 watts. This BBB on-board computer performs three functions: as a host, it signals the UWB module to send a ranging request; it also receives the distance measurement from the module; finally, it communicates the localization message as well as the path planning messages with Pixhawk through the interface board.

Fig. 6. P410 UWB platform.

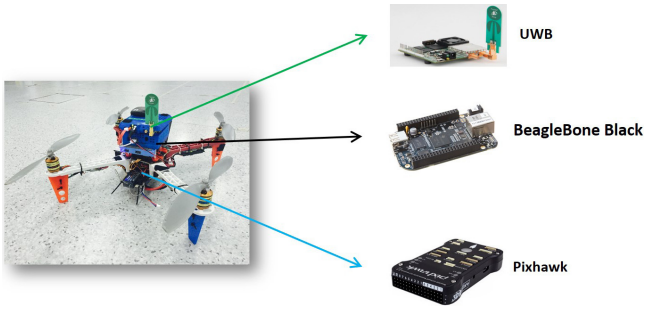

(a) System block diagrams

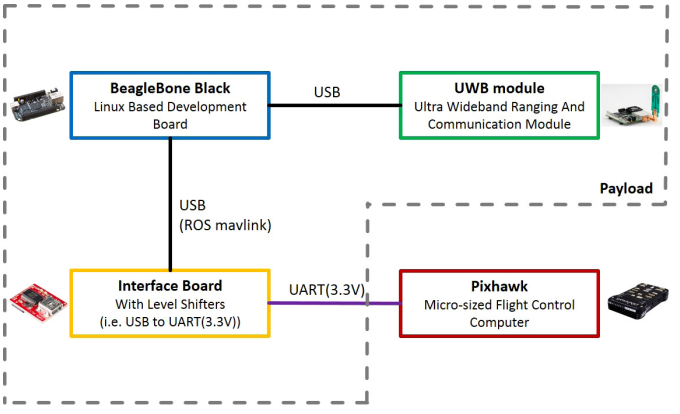

(b) Connection between components

Fig. 7. Hardware architecture.

The Pixhawk Autopilot is a high-performance autopilot-on-module suitable for different types of vehicles. It integrates the IMU and flight controller on-board. By default, it is connected to the GPS module for the absolute position, while in our case, it receives the localization message from BBB.

In addition, a micro radar sensor is installed to measure the relative altitude to the ground. The power of all the electronic components come from a 3-cell LiPo battery with capacity of 5200 mAh.

5. Experimental Results and Performance Evaluation

To validate the proposed UWB-based localization approach, various experiments have been conducted in different environments. Below, we shall discuss the experiments in detail. Particularly, the discussion is divided into 3 parts: range calibration, outdoor localization and indoor autonomous flight.

5.1. *Range calibration*

Considering that the calibration parameters in (3) may depend on the specific environment, the calibration of UWB measurement is conducted in different environments. Typically, we do the experiments in 3 kinds of environments: indoor environment, semi-outdoor environment (corridor) and forest environment.

5.1.1. *Indoor calibration*

For the indoor calibration, experiments were carried out in the test bed of Internet of Things Lab (Fig. 8(a)), which covers an approximate area of 7 m $\times$ 7 m. Samples were collected every 0.5 m within the range of 8 m, with the ground truth provided by a VICON system, which reaches the mm-level accuracy. We found that the accuracy of UWB

(a) IoT lab indoor environment

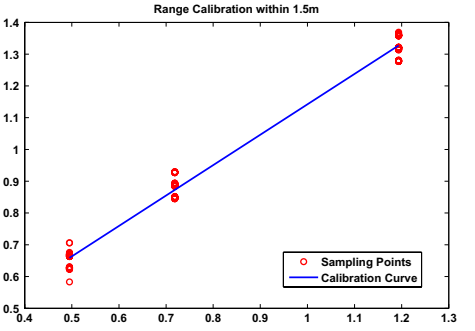

(b) IoT lab calibration $<$ 1.5 m

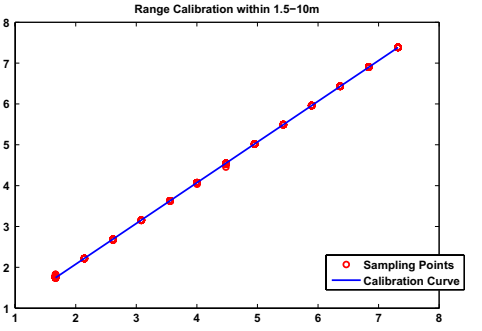

(c) IoT lab calibration 1.5–8 m

Fig. 8. Indoor range calibration and experimental results.

Table 1. Indoor Range Calibration (unit: m).

Range	$\tilde{a}$	$\tilde{b}$	STD after calibration	STD before calibration
0–1.5 m	1.0447	−0.1932	**0.032**	0.156
1.5–10 m	1.0029	−0.0829	**0.010**	0.069

measurement decreases significantly within 1.5 m, and hence separated the calibration into 2 intervals, 0–1.5 m and 1.5–8 m. As mentioned in Sec. 2.2, we first did the linear regression for the samples (Fig. 8(b) and 8(c)) and then got the calibration equation of (3). The parameters of the calibration are listed in Table 1.

5.1.2. *Semi-outdoor calibration*

For the semi-outdoor calibration, experiments were carried out over the corridor of building S1, level B4 in Nanyang Technological University (Fig. 9(a)), which consists of a long track of about 100 m. Samples were collected every 5 m within the range of 100 m, with the ground truth provided by a laser distance meter (Fluke 424D), which reaches the mm-level accuracy. We found that the accuracy of UWB measurement degrades after 50 m, and hence separated the calibration into 2 intervals, 10–50 m and 50–100 m. As mentioned in Sec. 2.2, we first did the linear regression for the samples (Figs. 9(b) and 9(c)) and then got the calibration equation of (3). The parameters of the calibration are listed in Table 2.

5.1.3. *Outdoor calibration*

For the outdoor calibration, experiments were carried out inside a woods in Nanyang Technological University (Fig. 10(a)), which covers an approximate area of 40 m × 30 m. Samples were collected at different locations along a 50 m long line-of-sight with the ground truth provided by the laser distance meter. The parameters of the calibration are listed in Table 3.

From Tables 1, 2 and 3, we can see that the UWB ranging is robust to the change of environments; actually, the largest standard error in 3 different environments is 0.061 m. However, the data loss and outliers increase with the distance, and vary in different environments. As expected, the data loss and outliers occur most in the forest environment. The prediction based on EKF can be used to continue operating for a system in the case of short-term measurement failures. The outliers applied directly can result in erratic estimation followed by large maneuvers and even crash during autonomous flight. Moreover, imprecise measurements without calibration will reduce the localization

(a) Corridor semi-indoor environment

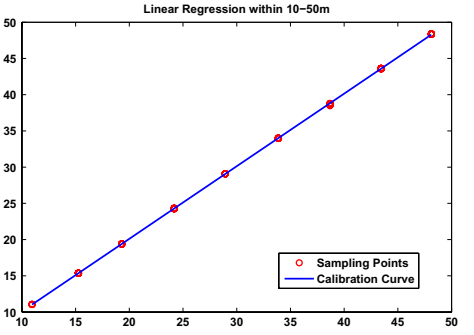

(b) Corridor calibration 10–50 m

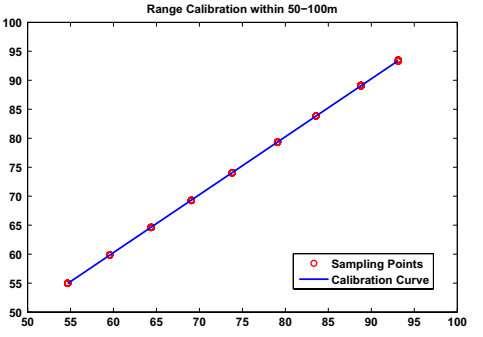

(c) Corridor calibration 50–100 m

Fig. 9. Semi-outdoor range calibration and experimental results.

accuracy and influence the performance of flight trajectory. Thus the calibration should be necessary before applying the raw range measurements. Figure 11 illustrates the outlier-removed and calibrated distance measurements are much closer to the reference than the raw distances at

Table 2. Semi-outdoor range calibration (unit: m).

Range	$\tilde{a}$	$\tilde{b}$	STD after calibration	STD before calibration
10–50 m	0.9976	−0.0511	**0.061**	0.675
50–100 m	1.0007	−0.3121	**0.046**	0.259

(a) Forest outdoor environment

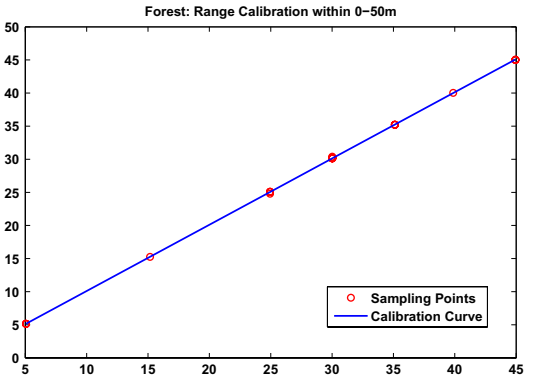

(b) Forest calibration 0–50 m

Fig. 10. Forest outdoor range calibration and experimental results.

Table 3. Outdoor range calibration (unit: m).

Range	$\tilde{a}$	$\tilde{b}$	STD after calibration	STD before calibration
0–50 m	0.9989	−0.0847	**0.054**	0.576

9.84 m, 14.85 m and 24.70 m, respectively. Compared with the raw range measurements with the mean error of 15 cm, the mean error of calibrated measurements is around 2 cm.

5.2. *UWB localization in outdoor environment*

To validate the UWB localization algorithm in outdoor environment, flight tests were conducted in a sports field (Fig. 12(a)). Four UWB modules in the center of the field were installed as anchors, marked as 4 black crosses in Fig. 12(c). The ground anchors share the same local frame and their Cartesian coordinates are given by (0.0, 0.0, 0.32), (0.0, 30.6, 1.26), (55.85, 30.6, 0.29) and (55.85, 0.0, 1.75), respectively from anchor 1 to 4. We used the same laser

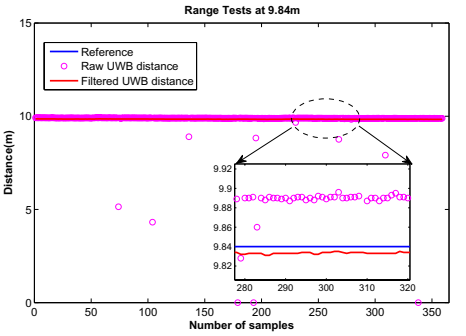

(a) Range tests at 9.84 m

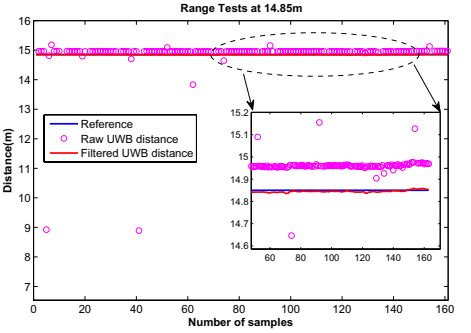

(b) Range tests at 14.85 m

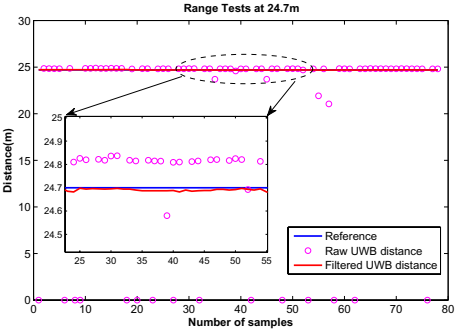

(c) Range tests at 24.7 m

Fig. 11. Performance of UWB ranging before and after calibration.

meter in Sec. 5.1 to determine the coordinates. To verify the performance of the proposed UWB-based localization, two tests were carried out. In the first experiment, the quadcopter was manually held overhead to move along the rectangle connecting the 4 anchors three times. Fig. 12(b) illustrates the UWB-based localization results, which almost overlap the rectangle. The average x–y error is 0.175 m with the worst case 0.32 m at the corner of the testing area, where the quadcopter was just above an anchor.

The second experiment was carried out in the same area with the same configuration of anchors. The quadcopter was maneuvered by a pilot to firstly fly along the same rectangle, and then along the 400 m running track.

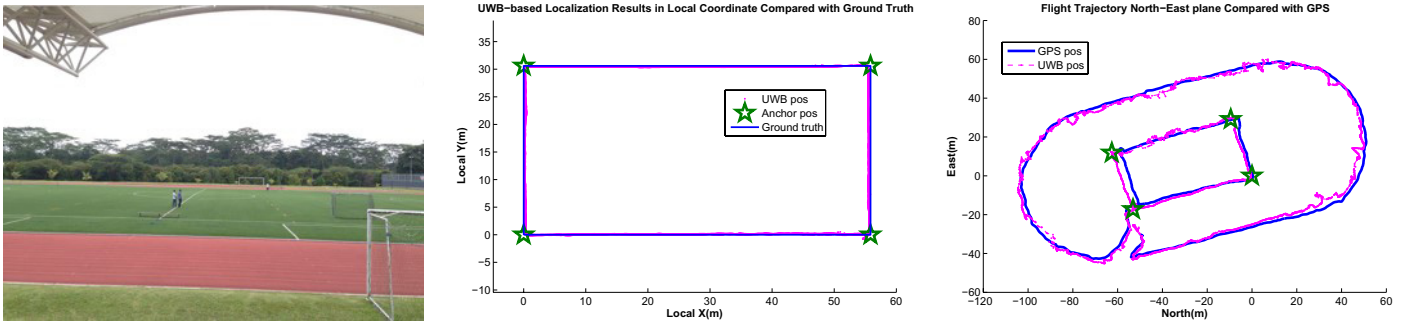

(a) Outdoor flight tests in SRC (b) Flight trajectory in North-East plane (c) Flight trajectory in North-East plane

Fig. 12. Performance of UWB outdoor localization compared with on-board GPS.

Figure 12(c) shows a comparison between the UWB estimate and the GPS estimate. Note that here the coordinate frame is taken as North–East plane, and the coordinates of the anchors have been rotated. As seen from the figure, the position estimate of UWB localization is closer to that of GPS, which is projected on the North–East plane from the GPS coordinates. In the outdoor case, it is difficult to retrieve the ground truth, especially when the UAV is moving, and hence we fail to conclude which estimate is more accurate than the other. But if we examine the rectangular path carefully, we can find that the deviation of the GPS estimate from the UWB estimate is different on the two opposite widths on North–West direction, which implies a better accuracy of the UWB localization than the GPS. On the other hand, we should also note that the UWB estimation degrades much on two arches, where the protective net for hammer-throw has been installed nearby. These metal materials result in more data loss and outliers as well as a decreased accuracy of UWB localization.

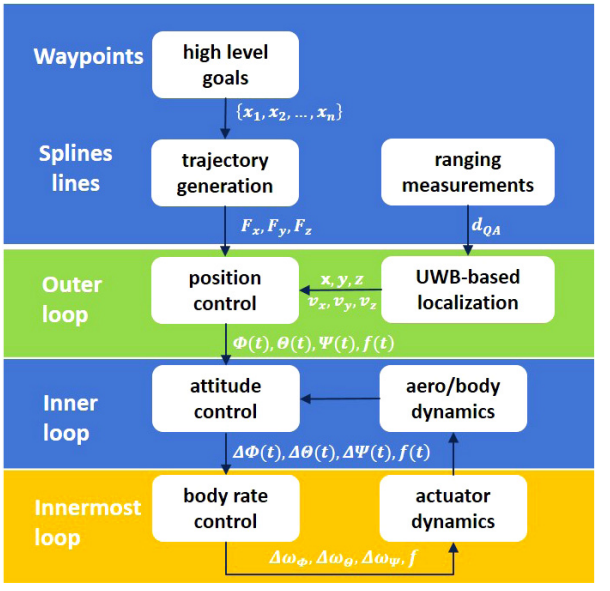

Fig. 13. Indoor autonomous flight workflow.

5.3. *Autonomous flight based on UWB localization in indoor environment*

To further validate the performance of UWB localization in indoor environment, we conducted an autonomous flight based on UWB localization in the same test bed as shown in Fig. 8(a). The quadcopter controllers can be modeled as a set of nested control loops as shown in Fig. 13. Each control loop has a reference set point and the current state as input. For the position control loop, the current state of the UAV is provided by the UWB-based localization module. The inner loop and innermost loop are carried out on Pixhawk Autopilot as shown in Fig. 7(a). The complete description of this design scheme can be seen in [34].

The UWB estimate is compared with the VICON measurements for the x–y coordinate and the corresponding velocity in Fig. 14. The commercial motion capture system (VICON) detects the pose of marked objects on the quadcopter and generates attitude and position information. All measurements are relative to a local coordinate frame. The system is capable of producing measurements at a rate of 200 Hz with position accuracy of millimeters. Similar to the setup in outdoor environment, four UWB modules were installed at the 4 corners of the test bed with the coordinates measured as $(-3.0, -3.0, -1.78)$, $(3.0, -3.0, -1.17)$, $(3.0, 3.0, -1.31)$ and $(-3.0, 3.0, -1.31)$, respectively, where the z-axis is taken downward.

The quadcopter takes off autonomously and flies around the center of the test bed three times in squarish trajectory. The position and velocity accuracy is affected by the Proportional-Integral-Derivative (PID) parameters and the precision of on-board magnetic sensor measurements, thus the flight trajectories do not overlap perfectly. However, the position and velocity estimates of UWB are quite close to those of VICON as shown in Fig. 14. The average position

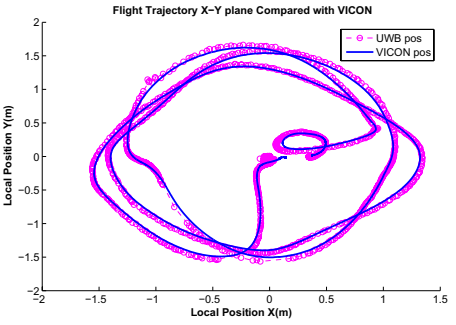

(a) Flight trajectory in x–y plane

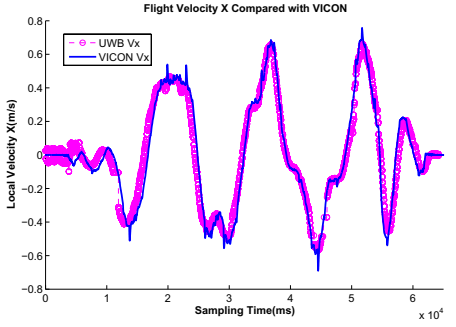

(b) Velocity x

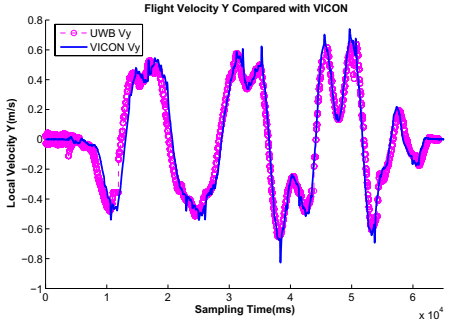

(c) Velocity y

Fig. 14. Comparison of UWB estimate and VICON measurement in indoor environment.

error in x–y plane is 0.071 m and in the worst case, the accuracy still falls within 0.2 m. For the velocity estimates in Figs. 14(a) and 14(b), the UWB estimation can track the dynamic movement of the quadcopter accurately. The estimation accuracy decreases at the turning points of trajectory, but it still falls within a reasonable range around the true value.

6. Conclusion and Future Work

The localization strategy proposed in this paper utilizes UWB radios to estimate the position and velocity of a flying quadcopter. Before a range measurement is fed into the localization algorithm, calibration and outlier detection are carried out for reliability and better accuracy. The proposed trilateration algorithm and EKF cooperate to achieve highly precise position and velocity estimates for autonomous flight of the quadcopter. Various experiments have been conducted in indoor and outdoor environments to validate the performance of the proposed UWB-based localization, and it shows that it is able to provide accurate position and velocity for the quadcopter navigation.

Future works will be steered to extend the set of sensors integrating IMU and visual information from fast camera. Two and more quadcopters may implement formation flight in indoor and outdoor environments or even in cluttered environments like forest. The number of anchors covering desired area can be optimized and the selection of nodes for localization of each quadcopter can be decided dynamically according to its current position. Furthermore, ranging based cooperative localization and multi-agent control will be investigated based on UWB.

References

[1] P. Liu, A. Y. Chen, Y.-N. Huang, J.-Y. Han, J.-S. Lai, S.-C. Kang, T.-H. Wu, M.-C. Wen and M.-H. Tsai, A review of rotorcraft unmanned aerial vehicle (uav) developments and applications in civil engineering, *Smart Struct. Syst.* **13**(6) (2014) 1065–1094.

[2] J. Paneque-Gálvez, M. K. McCall, B. M. Napoletano, S. A. Wich and L. P. Koh, Small drones for community-based forest monitoring: An assessment of their feasibility and potential in tropical areas, *Forests* **5**(6) (2014) 1481–1507.

[3] S. M. Khan, Gnss multipath interference and mitigation for uavs in urban canyon environments, *Aeronautical Telecommunications Network: Advances, Challenges, and Modeling* (CRC Press, US, 2015), p. 137.

[4] C. Teuliere, E. Marchand and L. Eck, 3-d model-based tracking for uav indoor localization, *IEEE Trans. Cybern.* **45**(5) (2015) 869–879.

[5] G. J. Vachtsevanos and K. P. Valavanis, Military and civilian unmanned aircraft, in *Handbook of Unmanned Aerial Vehicles* (Springer, NY, 2015), pp. 93–103.

[6] J. Guo, Z. Wang, M. Zheng and Y. Wang, An approach for uav reconnaissance mission planning problem under uncertain environment, *Int. J. Imaging and Robot.* **14**(3) (2014) 1–15.

[7] A. Eves, T. P. Stewart, A. P. Gay, A. Kemp, M. Easey, R. Angel, N. Thomas and D. Pearce, Developing unmanned aerial vehicles for local and flexible environmental and agricultural monitoring (2014).

[8] A. Wada, T. Yamashita, M. Maruyama, T. Arai, H. Adachi and H. Tsuji, A surveillance system using small unmanned aerial vehicle (uav) related technologies, *NEC Tech. J.* **8**(1) (2015) 68–72.

[9] C. Deng, S. Wang, Z. Huang, Z. Tan and J. Liu, Unmanned aerial vehicles for power line inspection: A cooperative way in platforms and communications, *J. Commun.* **9**(9) (2014) 687–692.

[10] J. Straub, Unmanned aerial systems: Consideration of the use of force for law enforcement applications, *Technol. Soc.* **39** (2014) 100–109.

[11] N. Abdelkrim, N. Aouf, A. Tsourdos and B. White, Robust nonlinear filtering for ins/gps uav localization, *IEEE Conf. on 16th Mediterranean in Control and Automation* (2008), pp. 695–702.

[12] A. Nemra and N. Aouf, Robust ins/gps sensor fusion for uav localization using sdre nonlinear filtering, *IEEE Sens. J.* **10**(4) (2010) 789–798.

[13] S. Sohn, B. Lee, J. Kim and C. Kee, Vision-based real-time target localization for single-antenna gps-guided uav, *IEEE Trans. Aerosp. Electron. Syst.* **44**(4) (2008) 1391–1401.

[14] J. Tisdale, A. Ryan, Z. Kim, D. Törnqvist and J. K. Hedrick, A multiple uav system for vision-based search and localization, in *IEEE Conf. on American Control* (2008) pp. 1985–1990.

[15] S. Rady, A. Kandil and E. Badreddin, A hybrid localization approach for uav in gps denied areas, in *IEEE Int. Symp. System Integration (SII), 2011 IEEE/SICE* (2011) pp. 1269–1274.

[16] B. Singh, S. K. Sahoo and S. R. Pradhan, Performance evaluation of anchor-based range-based localization systems in wireless sensor networks, *Perform. Eval.* **52**(17) (2012).

[17] G. Mao, B. Fidan and B. D. Anderson, Wireless sensor network localization techniques, *Comput. Netw.* **51**(10) (2007) 2529–2553.

[18] H. Liu, H. Darabi, P. Banerjee and J. Liu, Survey of wireless indoor positioning techniques and systems, *IEEE Trans. Syst., Man, Cybern. C, Appl. Rev.* **37**(6) (2007) 1067–1080.

[19] S. Gezici, Z. Tian, G. B. Giannakis, H. Kobayashi, A. F. Molisch, H. V. Poor and Z. Sahinoglu, Localization via ultra-wideband radios: A look at positioning aspects for future sensor networks, *IEEE, Signal Process. Mag.* **22**(4) (2005) 70–84.

[20] M. R. Mahfouz, C. Zhang, B. C. Merkl, M. J. Kuhn and A. E. Fathy, Investigation of high-accuracy indoor 3-d positioning using uwb technology, *IEEE Trans. Microw. Theory Techn.* **56**(6) (2008) 1316–1330.

[21] A. Prorok, A. Arfire, A. Bahr, J. R. Farserotu and A. Martinoli, Indoor navigation research with the khepera iii mobile robot: An experimental baseline with a case-study on ultra-wideband positioning, in *IEEE Int. Conf. 2010 Indoor Positioning and Indoor Navigation (IPIN)*, (2010) pp. 1–9.

[22] D. C. Montgomery, E. A. Peck and G. G. Vining, *Introduction to Linear Regression Analysis*, Vol. 821 (John Wiley & Sons, 2012).

[23] J. Berkson, Estimation of a linear function for a calibration line; consideration of a recent proposal, *Technometrics* **11**(4) (1969) 649–660.

[24] R. E. Kalman, A new approach to linear filtering and prediction problems, *J. Fluids Eng.* **82**(1) (1960) 35–45.

[25] E. Wan and R. Van Der Merwe *et al.*, The unscented kalman filter for nonlinear estimation, in *Adaptive Systems for Signal Processing, Communications, and Control Symposium 2000. AS-SPCC. The IEEE 2000*, pp. 153–158. IEEE, 2000.

[26] M. Boutayeb, H. Rafaralahy and M. Darouach, Convergence analysis of the extended kalman filter used as an observer for nonlinear deterministic discrete-time systems, *IEEE Trans. Autom. Control* **42**(4) (1997) 581–586.

[27] T. W. Anderson, T. W. Anderson, T. W. Anderson and T. W. Anderson, *An Introduction to Multivariate Statistical Analysis*, Vol. 2 (Wiley New York, 1958).

[28] D. E. Manolakis, Efficient solution and performance analysis of 3-d position estimation by trilateration, *IEEE Trans. Aerosp. Electron. Syst.* **32**(4) (1996) 1239–1248.

[29] Y. Zhou, An efficient least-squares trilateration algorithm for mobile robot localization, *IEEE Int. Conf. Intelligent Robots and Systems, 2009. IROS 2009. IEEE/RSJ* (2009), pp. 3474–3479.

[30] F. Thomas and L. Ros, Revisiting trilateration for robot localization, *IEEE Trans. Robot.* **21**(1) (2005) 93–101.

[31] W. Navidi, W. S. Murphy and W. Hereman, Statistical methods in surveying by trilateration, *Comput. Stat. Data Anal.* **27**(2) (1998) 209–227.

[32] C. T. Kelley, *Iterative Methods for Optimization*, Vol. 10 (Siam, 1999).

[33] L. Meier, P. Tanskanen, L. Heng, G. H. Lee, F. Fraundorfer and M. Pollefeys, Pixhawk: A micro aerial vehicle design for autonomous flight using onboard computer vision, *Auton. Robots* **33**(1–2) (2012) 21–39.

[34] D. Mellinger, N. Michael and V. Kumar, Trajectory generation and control for precise aggressive maneuvers with quadrotors, in *Experimental Robotics* (Springer, 2014) pp. 361–373.